Clim. Past Discuss., 11, 1313–1341, 2015
www.clim-past-discuss.net/11/1313/2015/
doi:10.5194/cpd-11-1313-2015

Climate of the Past
Discussions
Open Access

Early warnings and missed alarms for abrupt monsoon transitions

Z. A. Thomas[1,2], F. Kwasniok[3], C. A. Boulton[2], P. M. Cox[3], R. T. Jones[2], T. M. Lenton[2], and C. S. M. Turney[1]

[1]Climate Change Research Centre and School of Biological, Earth & Environmental Sciences, University of New South Wales, Sydney, NSW 2052, Australia
[2]College of Life and Environmental Science, University of Exeter, Exeter, EX4 4RJ, UK
[3]College of Engineering, Mathematics and Physical Sciences, University of Exeter, Exeter, EX4 4QF, UK

Received: 23 March 2015 – Accepted: 28 March 2015 – Published: 13 April 2015

Correspondence to: Z. A. Thomas (z.thomas@unsw.edu.au)

Published by Copernicus Publications on behalf of the European Geosciences Union.

Abstract

Palaeo-records from China (Cheng et al., 2009; Wang et al., 2008, 2001) demonstrate the East Asian Summer Monsoon (EASM) is dominated by abrupt and large magnitude monsoon shifts on millennial timescales, switching between periods of high and weak monsoon rains. It has been hypothesised that over these timescales, the EASM exhibits two stable states with bifurcation-type tipping points between them (Schewe et al., 2012). Here we test this hypothesis by looking for early warning signals of past bifurcations in speleothem records from Sanbao Cave and Hulu Cave, China (Wang et al., 2008, 2001), spanning the penultimate glacial cycle, and in multiple model simulations derived from the data. We find hysteresis behaviour in our model simulations with transitions directly forced by solar insolation. We detect critical slowing down prior to an abrupt monsoon shift during the penultimate deglaciation consistent with long-term orbital forcing. However, such signals are only detectable when the change in system stability is sufficiently slow to be detected by the sampling resolution of the dataset, raising the possibility that the alarm was missed and a similar forcing drove earlier EASM shifts.

1 Introduction

The Asian Summer Monsoon directly influences over 60 % of the world's population (Wu et al., 2012) and yet the drivers of past and future variability remain highly uncertain (Levermann et al., 2009; Zickfeld et al., 2005). Evidence based on radiometrically-dated speleothem records of past monsoon behaviour from East Asia (Yuan et al., 2004) suggests that on millennial timescales, the EASM is driven by a 23 kyr precession cycle (Kutzbach, 1981; Wang et al., 2008), but also influenced by feedbacks in sea surface temperatures and Northern Hemisphere ice volume (An, 2000). The demise of Chinese dynasties have been linked to monsoon shifts over more recent millennia (Zhang et al., 2008), suggesting that future changes, whether caused by solar or an-

CPD
11, 1313–1341, 2015

thropogenic forcing, could have similarly devastating societal impacts. Strikingly, the response of the monsoon to insolation changes is clearly not linear (Fig. 1); whilst Northern Hemisphere Summer Insolation (NHSI) follows a quasi-sinusoidal cycle, the $\delta^{18}O$ profile in speleothems exhibits a step function, suggesting the presence of threshold behaviour in the monsoon system (Schewe et al., 2012).

A minimum conceptual model (Levermann et al., 2009; Schewe et al., 2012) shows a non-linear solution structure with thresholds for switching a monsoon system between "on" or "off" states that can be defined in terms of atmospheric humidity – in particular, atmospheric specific humidity over the adjacent ocean (Schewe et al., 2012). Crucially, the presence of a critical threshold at the transition between the strong and weak regimes of the EASM means that early warning signals related to "critical slowing down" (Dakos et al., 2008; Lenton et al., 2012) could be detectable in suitable proxy records. Early warning signs of impending tipping points that are characterised by a bifurcation (rather than a noise-induced or rate-induced tipping e.g. Ashwin et al., 2012) can be mathematically detected by looking at the pattern of fluctuations in the short-term trends of a time-series before the transition takes place. A phenomenon called "critical slowing down" occurs on the approach to a tipping point, whereby the system takes longer to recover from small perturbations (Dakos et al., 2008). This longer recovery rate causes the intrinsic rates of change in the system to decrease, which is detected as a short-term increase in the autocorrelation of the time-series (Ives, 1995), often accompanied by an increasing trend in variance (Lenton et al., 2012). Detecting the phenomenon of critical slowing down relies on a timescale separation, whereby the timescale forcing the system is much slower than the timescale of the system's internal dynamics, which is in turn much longer than the frequency of data sampling the system. Although efforts have been taken to reduce the chances of type I and type II errors by correct pre-processing of data e.g. (Lenton, 2011), totally eradicating the chances of false positive and false negative results remains a challenge (Dakos et al., 2014; Lenton et al., 2012; Scheffer, 2010).

CPD
11, 1313–1341, 2015

Highly-resolved (~ 10^2 years) and precisely dated speleothem records of past monsoonal variability are well placed to test for early warning signals. The use of speleothem-based proxies to reconstruct patterns of palaeo-monsoon changes has increased rapidly over recent decades with the development of efficient sampling and dating techniques. However, there is currently some debate surrounding the climatic interpretation of Chinese speleothem $\delta^{18}O$ records (An et al., 2015), which can be influenced by competing factors that influence isotope fractionation. The oxygen isotopic composition of speleothem calcite is widely used to reconstruct palaeohydrological variations due to the premise that speleothem calcite $\delta^{18}O$ records the stable isotopic content of precipitation which has been shown to be inversely correlated with precipitation amount (Lee and Swann, 2010; Dansgaard, 1964), a relationship known as the "amount effect". Although the $\delta^{18}O$ of speleothem calcite in China has traditionally been used as a proxy for the "amount effect" (Cheng et al., 2006, 2009; Wang, 2009; Wang et al., 2008), this has been challenged by other palaeo-wetness proxies, notably (Maher, 2008) who argues that speleothems may be influenced by changes in rainfall source rather than amount. The influence of the Indian Monsoon has also been proposed as an alternative cause for abrupt monsoon variations in China (Liu et al., 2006; Pausata et al., 2011), though this has since been disputed (Liu et al., 2014; Wang and Chen, 2012). Importantly, however, robust replications of the same $\delta^{18}O$ trends in speleothem records across the wider region suggest they principally represent changes in the delivery of precipitation $\delta^{18}O$ associated with the EASM (Cheng et al., 2009, 2012; Duan et al., 2014; Li et al., 2013; Liu et al., 2014).

2 Methods

To investigate past tipping points in the behaviour of the EASM, we investigated past $\delta^{18}O$ changes preserved in the Sanbao Cave (Wang et al., 2008) and Hulu Cave (Wang et al., 2001) speleothems. It has been suggested that the EASM system responds specifically to 65° N 21 July insolation with a "near-zero phase lag" (Ruddiman, 2006).

CPD
11, 1313–1341, 2015

However, given that EASM development is affected by both remote and local insolation forcing (Liu et al., 2006), we use an insolation latitude local to the Sanbao record, consistent with earlier studies from this and other speleothem sequences (Wang et al., 2001). Since the monthly maximum insolation shifts in time with respect to the precession parameter, the 30° N June insolation was used, though we acknowledge that the insolation changes of 65° N 21 July as used by Wang et al. (2008) are similar with regard to the timing of maxima and minima. Crucially, immediately prior to Termination II, the Chinese speleothem data (including Sanbao Cave) record a "Weak Monsoon Interval" between 135.5 and 129 ka BP (Cheng et al., 2009), suggesting a lag of approximately 6.5 kyr following Northern Hemisphere summer insolation (Fig. 1).

2.1 Data selection

To test the proposed conceptual model of Schewe et al. (2012), we investigated the mechanisms behind abrupt shifts in the EASM over the penultimate glacial cycle (Marine Isotope Stage 6) using the Chinese speleothem record from Sanbao Cave (31°40′ N, 110°26′ E) (Wang et al., 2008), and Hulu Cave (32°30′ N, 119°10′ E) (Wang et al., 2001), considering both potential external and internal drivers. Some of the particular strengths of speleothem δ^{18}O as a record of past climate are their long duration (10^3–10^4 years), high-resolution and very precise and absolute-dated chronologies, making them ideal for tipping point analysis. Sanbao Cave in central China (speleothem SB11) and Hulu Cave in eastern China (speleothem MSP) have two of the highest resolution chronologies in the time period of interest, with a relatively constant density of data points, and provide some of the best records of Quaternary-scale monsoonal variation. Speleothem SB11 has one of the longest, continuous δ^{18}O records in China, with a very well constrained chronology and a temporal resolution of around 100 years (Wang et al., 2008) and is the only speleothem where analysis over an entire glacial cycle has been reported without using a spliced record. Speleothem MSP has a comparable resolution and density to SB11, though is significantly shorter. Crucially, the cave systems lie within two regionally distinct areas (Fig. 2), indicating that parallel

CPD
11, 1313–1341, 2015

changes in $\delta^{18}O$ cannot be explained by local effects. Tipping point analysis involves specific data requirements; not only does the data have to present a clear climate proxy, it also must be of an adequate length and resolution. In addition, since time series analysis methods require interpolation to equidistant data points, a relative constant density of data points is important. Figures 4 and 5 show that density of data points do not change significantly over either records, and thus the observed trends in autocorrelation are not an artefact of the data interpolation.

2.2 Tipping point analysis

A search for early warning signals of a bifurcation at each monsoon transition was carried out during each stable period (determined by deviation from the mean) between 230–128 ka BP of the Sanbao Cave speleothem record, and the shorter duration of the Hulu Cave speleothem record. Data pre-processing involved removal of long term trends using a Gaussian kernel smoothing filter and interpolation to ensure that the data is equidistant (a necessary assumption for time-series analysis), before the trends in autocorrelation and variance (using the R functions acf() and var() respectively) are measured over a sliding window of half the data length (Lenton et al., 2012). The smoothing bandwidth was chosen such that long-term trends were removed, without overfitting the data. A sensitivity analysis was undertaken by varying the size of the smoothing bandwidth and sliding window to ensure the results were robust over a range of parameter choices. Autocorrelation and variance are expected to increase on the approach to a bifurcation due to a gradual decrease in recovery rate to perturbations (Dakos et al., 2008; Lenton et al., 2012), based on the concept of critical slowing down. This phenomenon is fundamentally inherent to all bifurcational tipping points; when the system approaches a bifurcation point, the basin of attraction becomes wider and shallower, thus causing an increasingly slower characteristic return time to equilibrium (van Nes and Scheffer, 2007). This is measured through the autocorrelation or "memory" of a time series, and variance, which tracks the distance travelled from equi-

CPD
11, 1313–1341, 2015

librium. While it has been theoretically established that autocorrelation and variance should both increase together (Ditlevsen and Johnsen, 2010; Thompson and Sieber, 2011), there are some factors which can negate this, discussed in detail in Dakos et al. (2012, 2014).

The nonparametric Kendall's tau rank correlation coefficient was applied (Dakos et al., 2008) to test for statistical dependence for a sequence of measurements against time, varying between +1 and −1, describing the sign and strength of any trends in autocorrelation and variance. In addition, the results were tested against surrogate time series to ascertain the significance level of the results found, based on the null hypothesis that the data are generated by a stationary Gaussian linear stochastic process. The surrogate time series were generated by randomising the original data over 1000 permutations, which is sufficient to adequately estimate the probability distribution of the null model, and destroys the linear correlation while retaining the amplitude distribution of the original time series. Tipping point analysis was undertaken on these permutations, and a histogram constructed from the Kendall Tau values of autocorrelation and variance. The 90th and 95th percentiles provided the 90 and 95 % rejection thresholds respectively.

2.3 Non-stationary potential analysis

To supplement the analysis of the speleothem records and help interpret the results, a simple model derived directly from this data was constructed. Non-stationary potential analysis (Kwasniok, 2013) is a method for deriving from time series data a simple dynamical model which is modulated by external factors, here solar insolation. The dynamics of the monsoon system are conceptually described as motion in a time-dependent one-dimensional potential landscape; the influence of unresolved spatial and temporal scales is accounted for by stochastic noise. The shape of the potential as well as the noise level, are estimated from data in a maximum likelihood framework. The analysis allows for the detection of multi-stability in the system and helps pinpoint

CPD
11, 1313–1341, 2015

basic dynamical mechanisms, for example, directly forced vs. noise-induced transitions.

Simple statistical-dynamical models modulated by external factors are derived from data according to the maximum likelihood principle. The method allows extraction of basic dynamical mechanisms and to distinguish between competing dynamical explanations. We assume here that the monsoon system is governed by the effective one-dimensional Langevin equation:

$$\dot{x} = -V'(x;t) + \sigma\eta$$

where η is a white Gaussian noise process with zero mean and unit variance, and σ is the amplitude of the stochastic forcing. The potential landscape $V(x;t)$ is time-dependent, linearly modulated by the solar insolation:

$$V(x;t) = U(x) + \alpha I(t)x$$

The time-independent part of the potential, $U(x)$, is modelled by a fourth-order polynomial, allowing for possible bi-stability (Kwasniok and Lohmann, 2009). $I(t)$ is the insolation forcing and α is a coupling parameter. The model variable x is identified with the speleothem record. The model incorporates the possibility of directly forced transitions between the two states as well as noise-induced switching, including the phenomenon of stochastic resonance. The deterministic model parameters are estimated using only the probability density of the data (Kwasniok, 2013) rather than transition probabilities. This more generic approach takes account of the fact that the degree of validity of the model is not known a priori. The noise level is then estimated from the residuals. Inspection of the estimated model parameters enables assessment of the significance of the different mechanisms.

Having derived a model from the data, 100 realisations were analysed to test whether early warning signals could be detected in the model output. Sampling the same time series at different resolutions and noise levels allows us to explore the effect of these on the early warning signals. Accordingly, the model was manipulated by changing both

CPD
11, 1313–1341, 2015

the noise level and sampling resolution. To enable a straightforward comparison of the rate of forcing and the sampling resolution we linearized the solar insolation using the minimum and maximum values of the solar insolation over the time span of the model. To detrend the time series data, we ran the model without any external noise forcing to obtain the equilibrium solution to the system, which we then subtracted from the time series which did include noise. In addition, we manipulated the noise level of the model because the noise level in the original time series was too large to detect the movement towards the bifurcation. The time step in the series was reduced so that 6000 time points were available prior to the bifurcation and to ensure no data from beyond the tipping point was included in the analysis. Importantly, it is the movement toward the bifurcation rather than the distance from it that the early warning signals detect. Sampling the same time series at different resolutions allowed us to explore the effect of this on the early warning signals. When comparing early warning signals for differing sample steps and noise levels, the same iteration of the model was used to enable a direct comparison.

3 Results and discussion

A histogram of $\delta^{18}O$ values suggests that there are two modes in the EASM between 230–128 ka BP, as displayed by the double peak structure in Fig. 3a, supporting a number of studies that observe bimodality in tropical monsoon systems (Schewe et al., 2012; Zickfeld et al., 2005). To investigate further the dynamical origin of this bimodality we applied non-stationary potential analysis (Kwasniok, 2013). A non-stationary potential model was fitted, modulated by the solar forcing (NHSI June 30° N), covering the possibility of directly forced transitions as well as noise-induced transitions with or without stochastic resonance. This showed a bi-stable structure to the EASM with hysteresis (Figs. 3 and 4), suggesting that abrupt monsoon transitions may involve underlying bifurcations.

CPD
11, 1313–1341, 2015

Importantly, we found a clear increasing trend in both autocorrelation and variance covering data spanning the period 150 to 129 ka BP in the Sanbao Cave record, before Monsoon Termination II (Fig. 5). These proportional positive trends in both autocorrelation and variance are consistent with critical slowing down on the approach to a bifurcation (Ditlevsen and Johnsen, 2010). Furthermore, a sensitivity analysis was performed to ensure that the results were robust over a range of parameters by running repeats of the analysis with a range of smoothing bandwidths used to detrend the original data (5–15 % of the time series length) and sliding window sizes in which indicators are estimated (40–60 % of the time series length). The Kendall tau values are over 0.8 for the vast majority of smoothing bandwidth and sliding window sizes (Fig. 8). To test for significance, surrogate datasets were created by randomising each section of the original data over several thousand permutations (see Sect. 2.2 for more details). The AR(1) and variance for the original and each of the surrogate time series was computed, and the statistical significance obtained for the original data by comparing against the probability distribution of the surrogate data. We find that the Kendall tau value for autocorrelation has a significance level of $p < 0.05$ and for variance a significance level of $p < 0.1$ (Fig. 8).

To test whether the signal is present in other EASM records, we undertook the same analysis on a second speleothem sequence (Fig. 6), covering the same time period. We find that Speleothem MSP from Hulu Cave (32°30′ N, 119°10′ E) (Wang et al., 2001) displays a comparable increase in autocorrelation and variance to speleothem SB11 from Sanbao Cave (though these display slightly lower p values; see Fig. 9), suggesting our interpretation is robust. In contrast, the transitions during the earlier period 230–150 ka BP from Sanbao Cave have less consistent trends; although autocorrelation and variance do increase prior to some of the abrupt monsoon transitions, there is no clear evidence of critical slowing down across these transitions (see Fig. 10).

To help interpret these results we applied the potential model. In the model we find transitions occur under direct solar insolation forcing when reaching the end of the stable branches, explaining the high degree of synchronicity between the transitions

CPD
11, 1313–1341, 2015

and solar forcing. It is important to note that although the detection of early warning signals in time series data has been widely used for the detection of bifurcations in a range of systems (Dakos et al., 2008), there are instances when bifurcations are not preceded by critical slowing down. To explore this further, we initially produced an ensemble of 100 realisations of the potential model, looking for early warning signals prior to each transition (see Methods). We chose the sampling resolution of the model outputs to be comparable to the speleothem data (10^2 years). These 100 realisations appear broadly to follow the path of June insolation at 30° N with a small phase lag (Fig. 11). The model simulations also follow the speleothem palaeodata for all but the monsoon transition at 129 ka BP near Termination II, where the model simulations show no extended lag with respect to the insolation.

The results of the search for early warning signals in these 100 realisations of the model are plotted as histograms of the distribution of Kendall tau results for autocorrelation and variance (Fig. 11). In order to detect critical slowing down on the approach to a bifurcation, the data must capture the gradual flattening of the potential well. No consistent early warning signals were found in the period 230–129 ka BP, which we term "missed alarms" (Lenton et al., 2012). We suggest that these missed alarms are caused by a relatively fast rate of forcing compared to the sampling of the system; this comparatively poor sampling prevents the gradual flattening of the potential well from being recorded in the data. To test our hypothesis, we compared a range of different sampling time steps in the model (see Sect. 2.3) measuring the Kendall tau values of autocorrelation and variance over each realisation of the model (one realisation displayed in Fig. 12), which demonstrates the effects of increasing the sampling time step in the model. We found that whereas an increasing sampling time step produces a steady decrease in the Kendall tau values for AR(1) (Fig. 12b), Kendall tau values remain fairly constant for variance (Fig. 12c), suggesting that the latter is not affected by time step changes. This supports the contention by Dakos et al. (2012) that "high resolution sampling has no effect on the estimate of variance". In addition, we manipulated the noise level and found that decreasing the noise level by a factor of 2 was neces-

CPD
11, 1313–1341, 2015

sary to identify consistent early warning signals. This is illustrated in Fig. 12a, where the grey line represents the noise level as determined by the model, which does not follow a step transition, and cannot be adequately detrended by the equation derived from the model. However, once the noise level is sufficiently reduced, early warning signals (displayed here as high Kendall tau values for autocorrelation and variance) can be detected.

These results confirm that early warning signals may not be detected for bifurcations if the rate of forcing is too fast compared to the sampling rate, such that the flattening of the potential is poorly recorded in time series. "Missed alarms" may therefore be common in palaeodata where there is an insufficient sampling resolution to detect the flattening of the potential; a high sampling resolution is thus recommended to avoid this issue. There is more flattening visible in the potential for the monsoon transition at 129 ka BP (Termination II) which is due to the reduced amplitude of the solar forcing at the termination, but it is unclear whether this is sufficient to explain the early warning signal detected in the palaeodata. We suggest that additional forcing mechanisms may be driving the termination e.g. Caley et al. (2011) which cannot be captured by the potential model (as evidenced by the trajectory of the data falling outside the probability range of the potential model, Fig. 11). One possibility is continental ice volume effects may explain the presence of a longer lag between the change in insolation and the monsoon transition at glacial terminations (Cheng et al., 2009). Alternatively, reduced sea ice extent may have played a role (Wunch, 2006).

A Weak Monsoon Interval (WMI) in the EASM at 135.5–129 ka BP (Cheng et al., 2009) just prior to the glacial termination is thought to be linked to migrations in the Inter-tropical Convergence Zone (ITCZ) (Yancheva et al., 2007). Changes in the latitudinal temperature gradient (Rind, 1998) or planetary wave patterns (Wunsch, 2006) driven by continental ice volume (Cheng et al., 2009) and/or sea ice extent (Broccoli et al., 2006) may have played a role in causing this shift in the ITCZ. For instance, the cold anomaly associated with Heinrich event 11 (at 135 ka BP) has been invoked as a possible cause of the WMI, cooling the North Atlantic and shifting the Polar front and

CPD
11, 1313–1341, 2015

Siberian high southwards, forcing an equatorward migration of westerly airflow across Asia (Broecker et al., 1985; Cai et al., 2015; Cheng et al., 2009). Such a scenario would maintain a low thermal gradient between the land and sea, causing the Weak Monsoon Interval and potentially suppressing a simple insolation response.

4 Conclusions

We detect a fold bifurcation structure in the EASM in data analysed over the penultimate glacial cycle. We find evidence of critical slowing down before the abrupt monsoon shift at Termination II (129 ka BP) in the palaeodata. However, we do not find consistent early warning signals of a bifurcation for the abrupt monsoon shifts in the period between 230–150 ka BP. Exploration of sampling resolution from our model suggests that the absence of robust critical slowing down signals in the palaeodata is due to a combination of rapid forcing and the insufficient sampling resolution, preventing the detection of the steady flattening of the potential that occurs before a bifurcation. We also find that there is a noise threshold at which early warning signals can no longer be detected. The early warning signal detected at Termination II in the palaeodata is likely due to the longer lag during the Weak Monsoon Interval, linked to cooling in the North Atlantic. This allows a steadier flattening of the potential associated with the stability of the EASM and thus enables the detection of critical slowing down. Our results have important implications for identifying early warning signals in other natural archives. One great advantage of the speleothems reported here is the detection of an early warning signal during one transition compared to previous events in the same record provides an insight into changing/additional forcing mechanisms. However, in records with a single abrupt shift, the failure to identify a critical slowing down does not preclude a bifurcation.

Acknowledgements. The data for this paper are available from the National Climate Data Centre, NOAA (SB11: http://hurricane.ncdc.noaa.gov/pls/paleox/f?p=519:1::P1_STUDY_ID:8641

CPD
11, 1313–1341, 2015

and Hulu: http://hurricane.ncdc.noaa.gov/pls/paleox/f?p=519:1::P1_STUDY_ID:5426). The authors declare no competing financial interests.

References

An, Z.: The history and variability of the East Asian paleomonsoon climate, Quaternary Sci. Rev., 19, 171–187, doi:10.1016/S0277-3791(99)00060-8, 2000.

An, Z., Guoxiong, W., Jianping, L., Youbin, S., Yimin, L., Weijian, Z., Yanjun, C., Anmin, D., Li, L., Jiangyu, M., Hai, C., Zhengguo, S., Liangcheng, T., Hong, Y., Hong, A., Hong, C., and Juan, F.: Global monsoon dynamics and climate change, Annu. Rev. Earth Pl. Sc., 43, 1–49, doi:10.1146/annurev-earth-060313-054623, 2015.

Ashwin, P., Wieczorek, S., Vitolo, R., and Cox, P.: Tipping points in open systems: bifurcation, noise-induced and rate-dependent examples in the climate system, Philos. T. R. Soc. A, 370, 1–20, doi:10.1098/rsta.2011.0306, 2012.

Berger, A. and Loutre, M. F.: Insolation values for the climate of the last 10 million years, Quaternary Sci. Rev., 10, 297–317, 1991.

Broccoli, A. J., Dahl, K. A., and Stouffer, R. J.: Response of the ITCZ to Northern Hemisphere cooling, Geophys. Res. Lett., 33, 1–4, doi:10.1029/2005GL024546, 2006.

Broecker, W. S., Peteet, D. M., and Rind, D.: Does the ocean–atmosphere system have more than one stable mode of operation?, Nature, 315, 21–26, 1985.

Cai, Y., Fung, I. Y., Edwards, R. L., An, Z., Cheng, H., Lee, J.-E., Tan, L., Shen, C.-C., Wang, X., Day, J. a., Zhou, W., Kelly, M. J., and Chiang, J. C. H.: Variability of stalagmite-inferred Indian monsoon precipitation over the past 252 000 years, ADDIN Mendeley Bibliography CSL_BIBLIOGRAPHY, Proc. Natl. Acad. Sci., 112, 2954–2959, doi:10.1073/pnas.1424035112, 2015.

Caley, T., Malaizé, B., Revel, M., Ducassou, E., Wainer, K., Ibrahim, M., Shoeaib, D., Migeon, S., and Marieu, V.: Orbital timing of the Indian, East Asian and African boreal monsoons and the concept of a "global monsoon," Quaternary Sci. Rev., 30, 3705–3715, doi:10.1016/j.quascirev.2011.09.015, 2011.

Cheng, H., Edwards, R. L., Wang, Y., Kong, X., Ming, Y., Kelly, M. J., Wang, X., Gallup, C. D., and Liu, W.: A penultimate glacial monsoon record from Hulu Cave and two-phase glacial terminations, Geology, 34, 217, doi:10.1130/G22289.1, 2006.

CPD
11, 1313–1341, 2015

Early warnings and missed alarms for abrupt monsoon transitions

Z. A. Thomas et al.

Cheng, H., Edwards, R. L., Broecker, W. S., Denton, G. H., Kong, X., Wang, Y., Zhang, R., and Wang, X.: Ice age terminations, Science, 326, 248–252, doi:10.1126/science.1177840, 2009.

Cheng, H., Sinha, A., Wang, X., Cruz, F. W., and Edwards, R. L.: The global paleomonsoon as seen through speleothem records from Asia and the Americas, Clim. Dynam., 39, 1045–1062, doi:10.1007/s00382-012-1363-7, 2012.

Dakos, V., Scheffer, M., van Nes, E. H., Brovkin, V., Petoukhov, V., and Held, H.: Slowing down as an early warning signal for abrupt climate change, P. Natl. Acad. Sci. USA, 105, 14308–14312, doi:10.1073/pnas.0802430105, 2008.

Dakos, V., van Nes, E. H., D'Odorico, P., and Scheffer, M.: Robustness of variance and autocorrelation as indicators of critical slowing down, Ecology, 93, 264–271, 2012.

Dakos, V., Carpenter, S. R., van Nes, E. H., and Scheffer, M.: Resilience indicators: prospects and limitations for early warnings of regime shifts, Philos. T. R. Soc. B, 370, 20130263, doi:10.1098/rstb.2013.0263, 2014.

Ditlevsen, P. D. and Johnsen, S. J.: Tipping points: early warning and wishful thinking, Geophys. Res. Lett., 37, L19703, doi:10.1029/2010GL044486, 2010.

Duan, F., Liu, D., Cheng, H., Wang, X., Wang, Y., Kong, X., and Chen, S.: A high-resolution monsoon record of millennial-scale oscillations during Late MIS 3 from Wulu Cave, southwest China, J. Quaternary Sci., 29, 83–90, doi:10.1002/jqs.2681, 2014.

Ives, A.: Measuring resilience in stochastic systems, Ecol. Monogr., 65, 217–233, doi:10.2307/2937138, 1995.

Kutzbach, J. E.: Monsoon climate of the early Holocene: climate experiment with the Earth's orbital parameters for 9000 years ago, Science, 214, 59–61, 1981.

Kwasniok, F.: Predicting critical transitions in dynamical systems from time series using nonstationary probability density modeling, Phys. Rev. E, 88, 052917, doi:10.1103/PhysRevE.88.052917, 2013.

Kwasniok, F. and Lohmann, G.: Deriving dynamical models from paleoclimatic records: application to glacial millennial-scale climate variability, Phys. Rev. E, 80, 066104, doi:10.1103/PhysRevE.80.066104, 2009.

Lenton, T. M.: Early warning of climate tipping points, Nat. Clim. Chang., 1, 201–209, doi:10.1038/nclimate1143, 2011.

CPD
11, 1313–1341, 2015

Lenton, T. M., Livina, V. N., Dakos, V., van Nes, E. H., and Scheffer, M.: Early warning of climate tipping points from critical slowing down: comparing methods to improve robustness, Philos. T. R. Soc. A, 370, 1185–204, doi:10.1098/rsta.2011.0304, 2012.

Levermann, A., Schewe, J., Petoukhov, V., and Held, H.: Basic mechanism for abrupt monsoon transitions, P. Natl. Acad. Sci. USA, 106, 20572–20577, doi:10.1073/pnas.0901414106, 2009.

Li, T.-Y., Shen, C.-C., Huang, L.-J., Jiang, X.-Y., Yang, X.-L., Mii, H.-S., Lee, S.-Y., and Lo, L.: Stalagmite-inferred variability of the Asian summer monsoon during the penultimate glacial–interglacial period, Clim. Past, 10, 1211–1219, doi:10.5194/cp-10-1211-2014, 2014.

Lisiecki, L. E. and Raymo, M. E.: A Pliocene–Pleistocene stack of 57 globally distributed benthic δ^{18}O records, Paleoceanography, 20, 1–17, doi:10.1029/2004PA001071, 2005.

Liu, X., Liu, Z., Kutzbach, J. E., Clemens, S. C., and Prell, W. L.: Hemispheric insolation forcing of the Indian Ocean and Asian Monsoon: local versus remote impacts, J. Climate, 19, 6195–6208, doi:10.1175/JCLI3965.1, 2006.

Liu, Z., Wen, X., Brady, E. C., Otto-Bliesner, B., Yu, G., Lu, H., Cheng, H., Wang, Y., Zheng, W., Ding, Y., Edwards, R. L., Cheng, J., Liu, W., and Yang, H.: Chinese cave records and the East Asia Summer Monsoon, Quaternary Sci. Rev., 83, 115–128, doi:10.1016/j.quascirev.2013.10.021, 2014.

Maher, B. A.: Holocene variability of the East Asian summer monsoon from Chinese cave records: a re-assessment, Holocene, 18, 861–866, doi:10.1177/0959683608095569, 2008.

Pausata, F. S. R., Battisti, D. S., Nisancioglu, K. H., and Bitz, C. M.: Chinese stalagmite δ^{18}O controlled by changes in the Indian monsoon during a simulated Heinrich event, Nat. Geosci., 4, 474–480, doi:10.1038/ngeo1169, 2011.

Petit, J. R., Raynaud, D., Basile, I., Chappellaz, J., Davisk, M., Ritz, C., Delmotte, M., Legrand, M., Lorius, C., Pe, L., and Saltzmank, E.: Climate and atmospheric history of the past 420,000 years from the Vostok ice core, Antarctica, Nature, 399, 429–436, 1999.

Rind, D.: Latitudinal temperature gradients and climate change, J. Geophys. Res., 103, 5943, doi:10.1029/97JD03649, 1998.

Ruddiman, W. F.: What is the timing of orbital-scale monsoon changes?, Quaternary Sci. Rev., 25, 657–658, doi:10.1016/j.quascirev.2006.02.004, 2006.

Scheffer, M.: Foreseeing tipping points, Nature, 467, 6–7, 2010.

Schewe, J., Levermann, A., and Cheng, H.: A critical humidity threshold for monsoon transitions, Clim. Past, 8, 535–544, doi:10.5194/cp-8-535-2012, 2012.

Thompson, J. and Sieber, J.: Predicting climate tipping as a noisy bifurcation: a review, Int. J. Bifurcat. Chaos, 21, 399–423, doi:10.1142/S0218127411028519, 2011.
Van Nes, E. H. and Scheffer, M.: Slow recovery from perturbations as a generic indicator of a nearby catastrophic shift, Am. Nat., 169, 738–47, doi:10.1086/516845, 2007.
Wang, H. and Chen, H.: Climate control for southeastern China moisture and precipitation: Indian or East Asian monsoon?, J. Geophys. Res.-Atmos., 117, D12109, doi:10.1029/2012JD017734, 2012.
Wang, P.: Global monsoon in a geological perspective, Chinese Sci. Bull., 54, 1113–1136, doi:10.1007/s11434-009-0169-4, 2009.
Wang, Y., Cheng, H., Edwards, R. L., Kong, X., Shao, X., Chen, S., Wu, J., Jiang, X., Wang, X., and An, Z.: Millennial- and orbital-scale changes in the East Asian monsoon over the past 224,000 years, Nature, 451, 18–21, doi:10.1038/nature06692, 2008.
Wang, Y. J., Cheng, H., Edwards, R. L., An, Z. S., Wu, J. Y., Shen, C. C., and Dorale, J. A.: A high-resolution absolute-dated late Pleistocene Monsoon record from Hulu Cave, China, Science, 294, 2345–2348, doi:10.1126/science.1064618, 2001.
Wu, G., Liu, Y., He, B., Bao, Q., Duan, A., and Jin, F.-F.: Thermal controls on the Asian summer monsoon, Sci. Rep., 2, 1–7, doi:10.1038/srep00404, 2012.
Wunsch, C.: Abrupt climate change: an alternative view, Quaternary Res., 65, 191–203, doi:10.1016/j.yqres.2005.10.006, 2006.
Yancheva, G., Nowaczyk, N. R., Mingram, J., Dulski, P., Schettler, G., Negendank, J. F. W., Liu, J., Sigman, D. M., Peterson, L. C., and Haug, G. H.: Influence of the intertropical convergence zone on the East Asian monsoon, Nature, 445, 74–77, doi:10.1038/nature05431, 2007.
Yuan, D., Cheng, H., Edwards, R. L., Dykoski, C. A., Kelly, M. J., Zhang, M., Qing, J., Lin, Y., Wang, Y., Wu, J., Dorale, J. A., An, Z., and Cai, Y.: Timing, duration, and transitions of the last interglacial Asian monsoon, Science, 304, 575–578, doi:10.1126/science.1091220, 2004.
Zhang, P., Cheng, H., Edwards, R. L., Chen, F., Wang, Y., Yang, X., Liu, J., Tan, M., Wang, X., Liu, J., An, C., Dai, Z., Zhou, J., Zhang, D., Jia, J., Jin, L., and Johnson, K. R.: A test of climate, sun, and culture relationships from an 1810-year Chinese cave record, Science, 322, 940–942, doi:10.1126/science.1163965, 2008.
Zickfeld, K., Knopf, B., Petoukhov, V., and Schellnhuber, H. J.: Is the Indian summer monsoon stable against global change?, Geophys. Res. Lett., 32, L15707, doi:10.1029/2005GL022771, 2005.

CPD
11, 1313–1341, 2015

Early warnings and missed alarms for abrupt monsoon transitions

Z. A. Thomas et al.

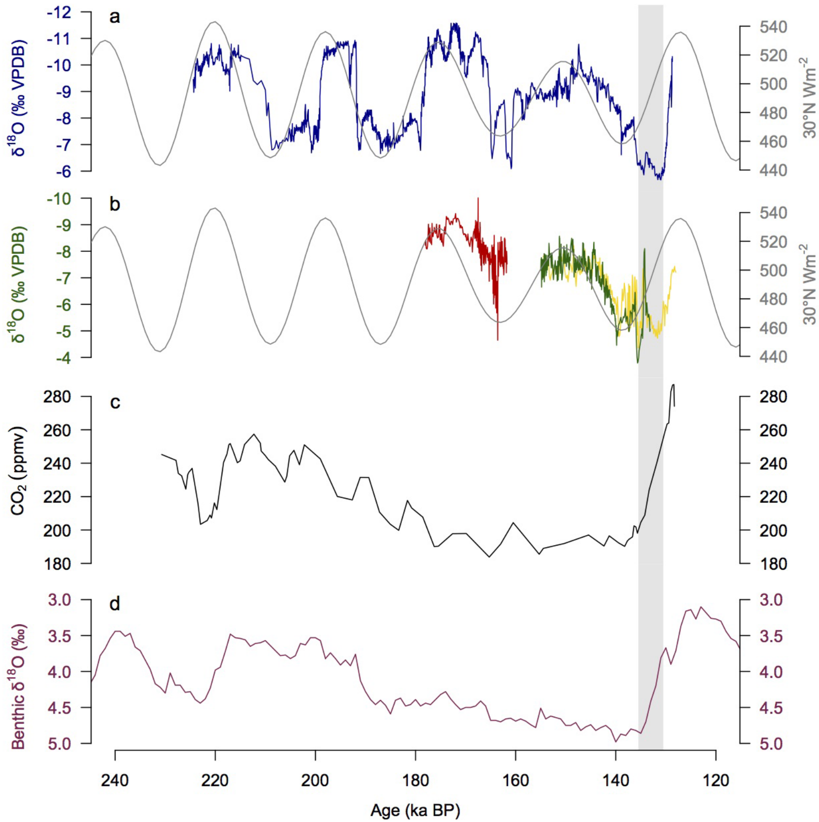

Figure 1. (a) Northern Hemisphere Summer Insolation (NHSI) at June 30° N (Berger and Loutre, 1991) (grey), δ^{18}O speleothem data from Sanbao Cave (Wang et al., 2008) (blue), **(b)** δ^{18}O speleothem data from Hulu Cave (Wang et al., 2001); speleothem MSH (red), MSP (green) and MSX (yellow), **(c)** CO_2 (ppmv) from the Antarctic Vostok ice core (Petit et al., 1999) (black), **(d)** δ^{18}O per mille benthic carbonate (Lisiecki and Raymo, 2005) (proxy for global ice volume) (purple).

CPD
11, 1313–1341, 2015

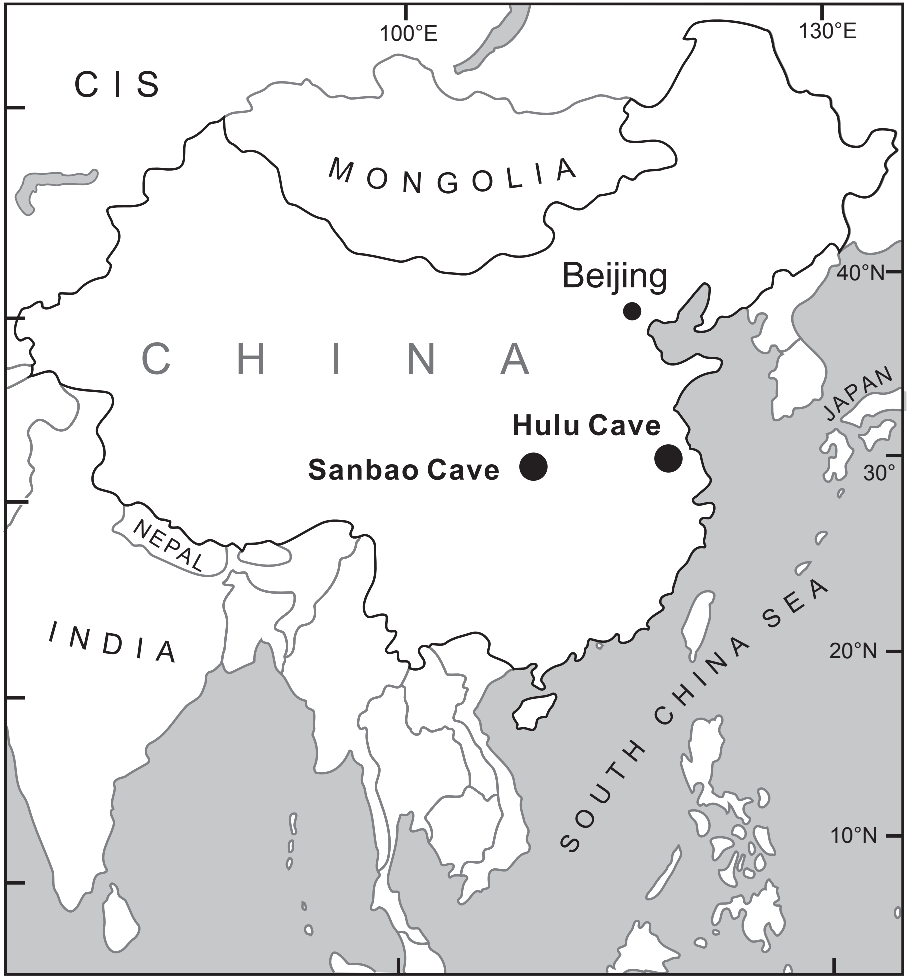

Figure 2. Map showing the location of Sanbao and Hulu caves.

CPD
11, 1313–1341, 2015

Early warnings and missed alarms for abrupt monsoon transitions

Z. A. Thomas et al.

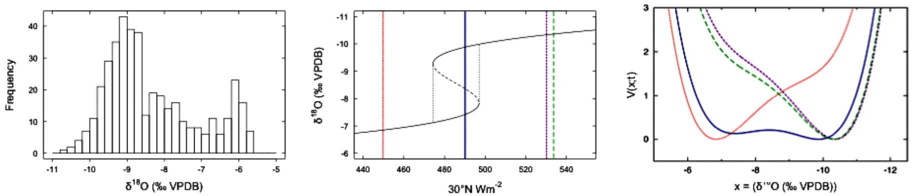

Figure 3. (a) Histogram showing the probability density of the speleothem data aggregated over 224–128 ka BP, **(b)** bifurcation diagram obtained from potential model analysis, showing bi-stability and hysteresis. Solid black lines indicate stable states, dotted line unstable states, and dashed vertical lines the jumps between the two stable branches. Coloured vertical lines correspond to the insolation values for which the potential curve is shown in **(c)**; **(c)** shows how the shape of the potential well changes over one transition cycle (198–175 ka BP) (green long dash = 535 W m^{-2}, purple short dash = 531 W m^{-2}, blue solid = 490 W m^{-2}, red dotted = 449 W m^{-2}) (for more details see Fig. 4).

CPD
11, 1313–1341, 2015

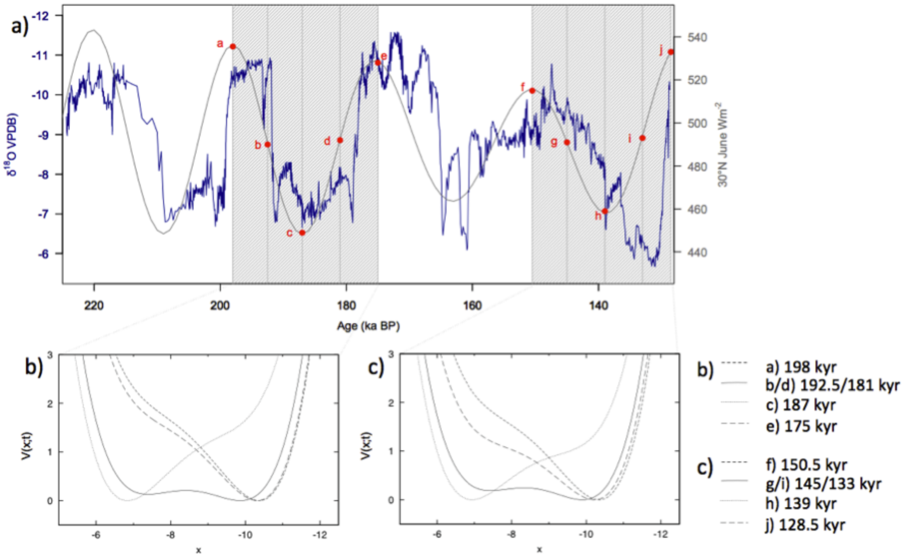

Figure 4. Potential analysis showing the changing shape of the potential well over **(b)** a normal transition cycle; and **(c)** the transition cycle at the termination. (Dotted lines show stages of the transition over high, medium, and low insolation values.) There is some visible flattening in the potential in panel **(c)** which is due to the reduced amplitude of the solar forcing at the termination

CPD
11, 1313–1341, 2015

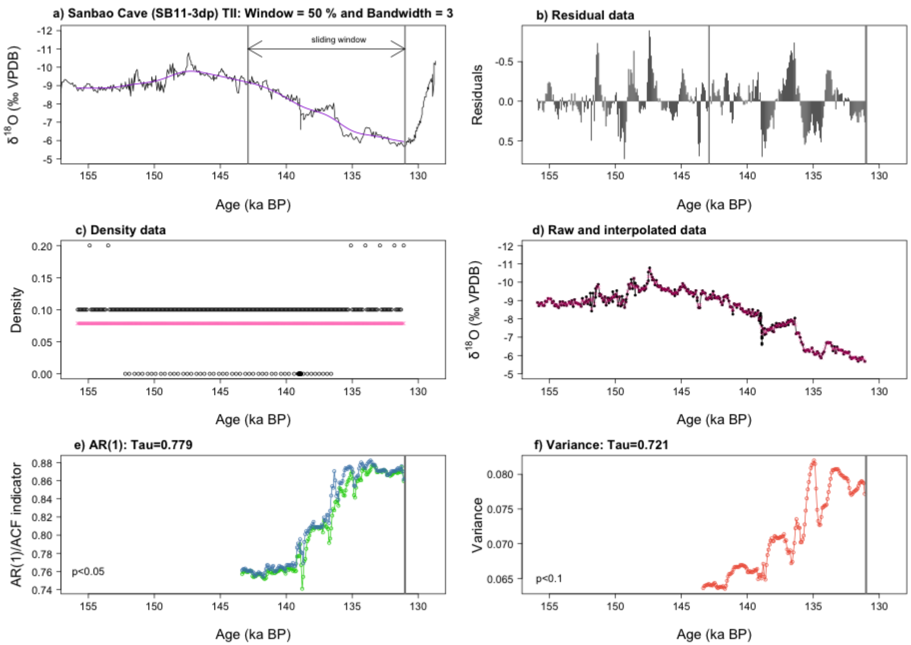

Figure 5. Tipping Point analysis on data from Sanbao Cave (Speleothem SB11) (31°40′ N, 110°26′ E). **(a)** Data was smoothed over an appropriate bandwidth (purple line) to produce data residuals **(b)**, and analysed over a sliding window (of size between the two grey vertical lines). The grey vertical line at 131 ka BP indicates the tipping point, and the point up to which the data is analysed. **(c, d)** Displays the data density, where the black points are the original data and the pink points are the data after interpolation. **(e)** Displays the AR(1) values and associated Kendall tau value, and **(f)** displays the variance and associated Kendall tau.

CPD
11, 1313–1341, 2015

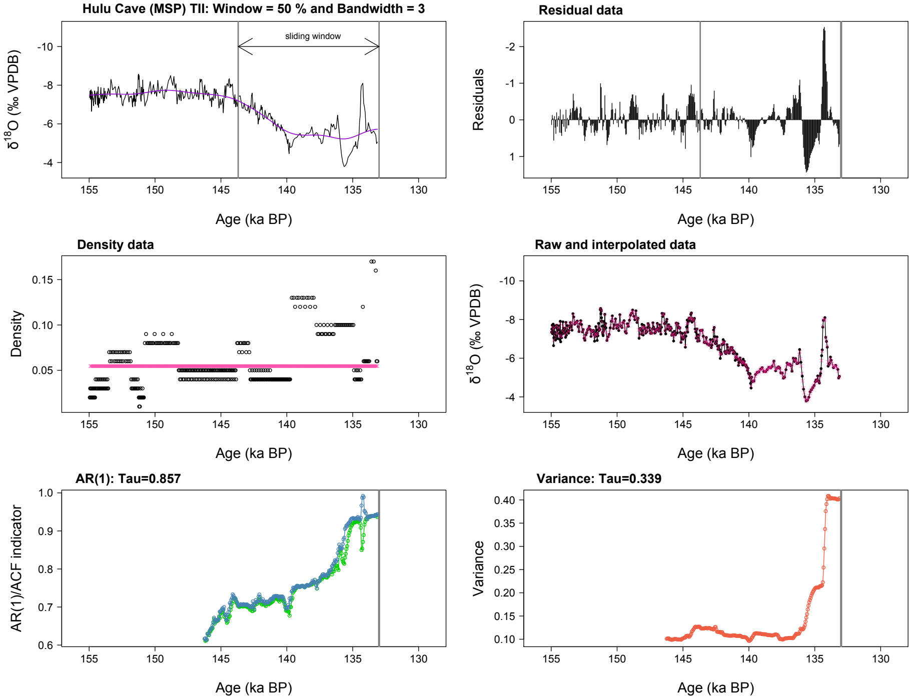

Figure 6. Tipping Point analysis on data from Hulu Cave (Speleothem MSP) (32°30′ N, 119°10′ E) **(a)** Data was smoothed over an appropriate bandwidth (purple line) to produce data residuals **(b)**, and analysed over a sliding window (of size between the two grey vertical lines). The grey vertical line at 131 kaBP indicates the tipping point, and the point up to which the data is analysed. **(c, d)** Displays the data density, where the black points are the original data and the pink points are the data after interpolation. **(e)** Displays the AR(1) values and associated Kendall tau value, and **(f)** displays the variance and associated Kendall tau.

CPD
11, 1313–1341, 2015

Discussion Paper | Discussion Paper | Discussion Paper | Discussion Paper |

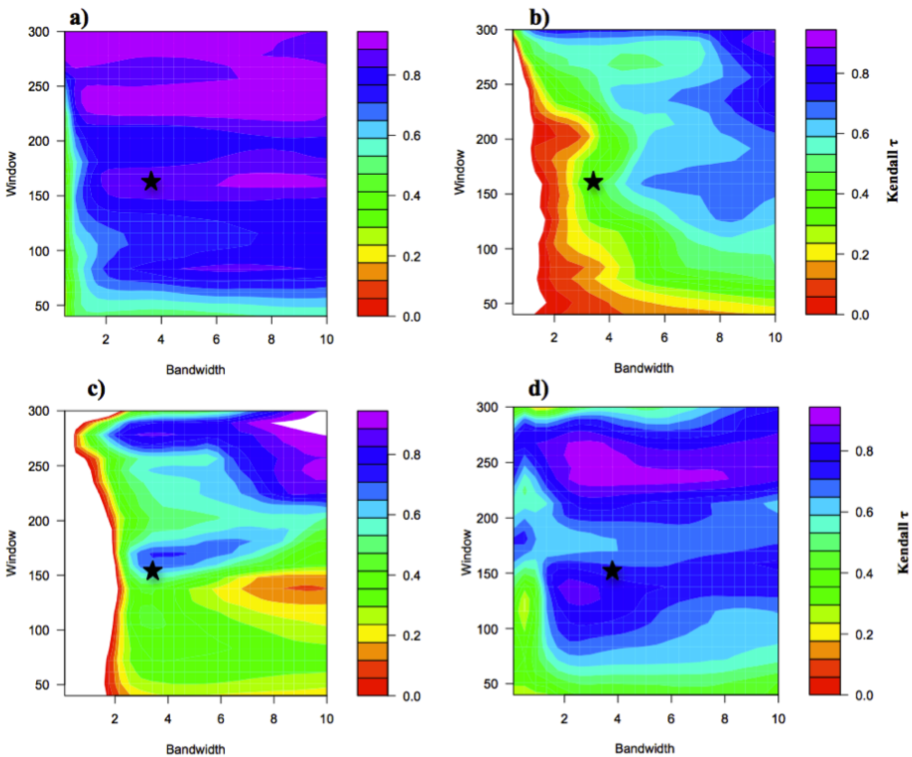

Figure 7. Contour plots showing a range of Window and Bandwidth sizes for the analysis; **(a)** Sanbao SB11 autocorrelation, **(b)** Sanbao SB11 variance, **(c)** Hulu MSP autocorrelation, **(d)** Hulu MSP variance. Black stars indicate the parameters used for the analysis in Figs. 5 and 6.

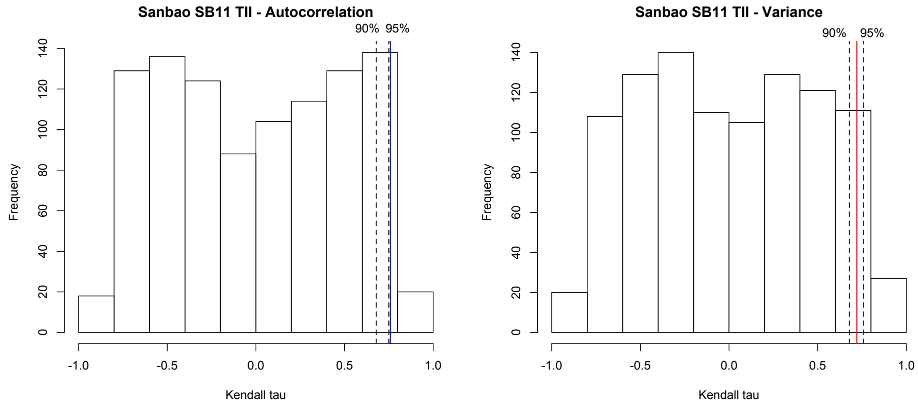

Figure 8. Histogram showing frequency distribution of Kendall tau values from 1000 realisations of a surrogate time series model. The grey dashed lines indicate the 90 and 95 % significance level and the blue and red vertical lines show the Kendall tau values from the original SB11 time series at Termination II for autocorrelation **(a)** and variance **(b)** respectively.

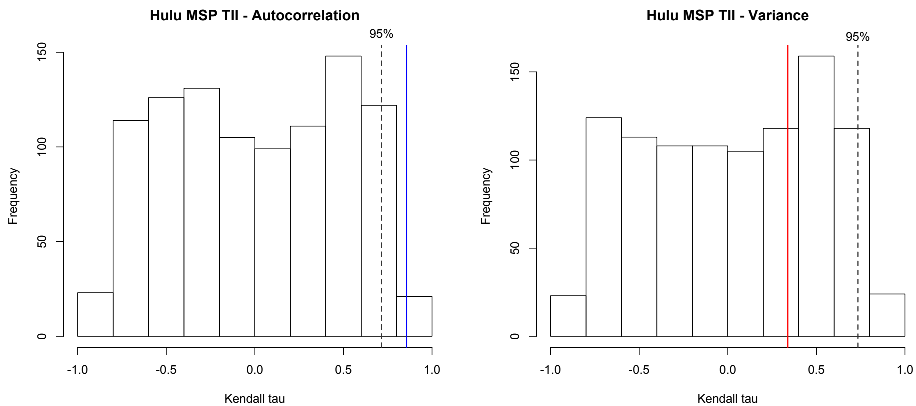

Figure 9. Histogram showing frequency distribution of Kendall tau values from 1000 realisations of a surrogate time series model. The grey dashed line indicate the 95 % significance level and the blue and red vertical lines show the Kendall tau values from the original Hulu MSP time series at Termination II for autocorrelation **(a)** and variance **(b)** respectively.

CPD
11, 1313–1341, 2015

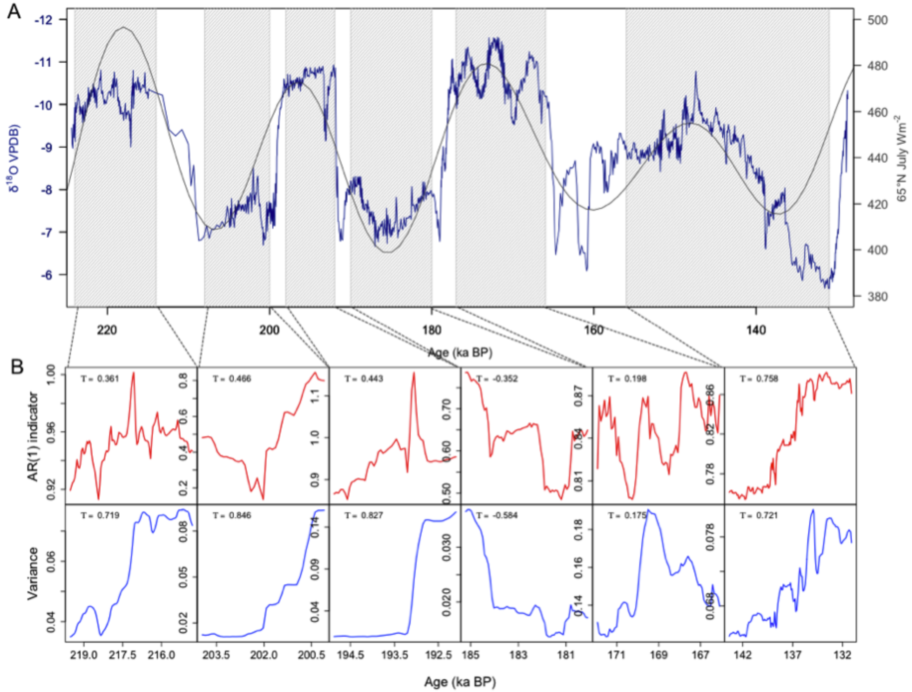

Figure 10. (a) δ^{18}O speleothem data from Sanbao Cave (SB11) (blue line) and NHSI at July 65° N (grey line). Grey hatched areas show the sections of data selected for tipping point analysis. **(b)** These panels show the corresponding autocorrelation and variance for each period prior to a transition. No values are annotated since it is the increasing trend, rather than the absolute values of the autocorrelation and variance that indicate critical slowing down. The colour legend shows the Kendall tau values (−1 to 1) from autocorrelation over a range of smoothing bandwidths (5–15 %) and sliding windows (40–60 % of data range).

CPD
11, 1313–1341, 2015

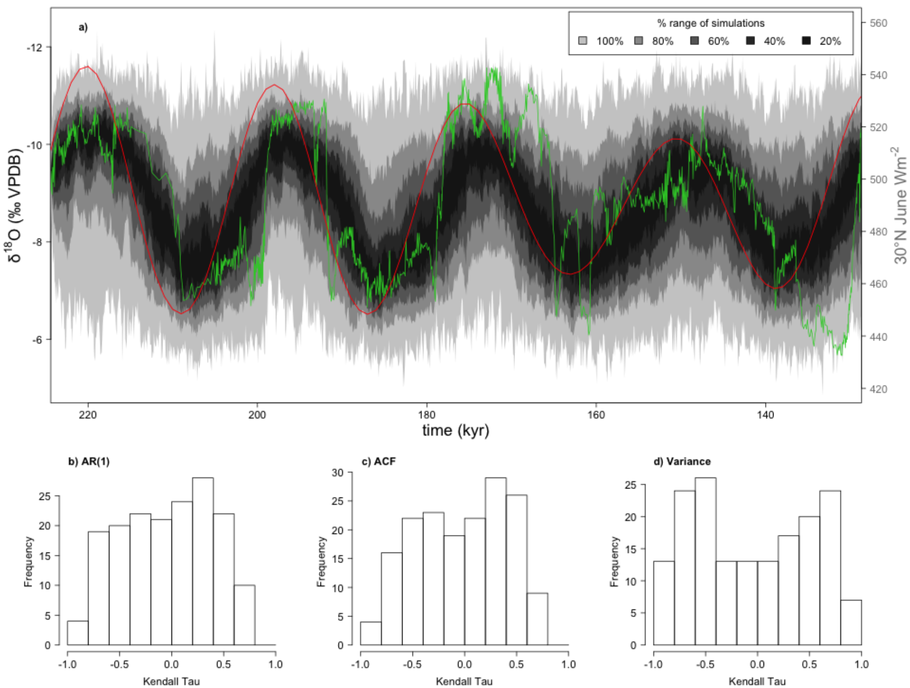

Figure 11. (a) Probability range of 100 model simulations, with the June 30° N NHSI (in red), and the palaeodata from SB11 (in green); histograms showing the distribution of the Kendall tau values from running the AR(1) **(b)**, ACF **(c)** and variance **(d)** over the monsoon transitions for the period 230–128 ka BP. Note there is no significant skewness associated with trends towards increased autocorrelation and variance.

CPD
11, 1313–1341, 2015

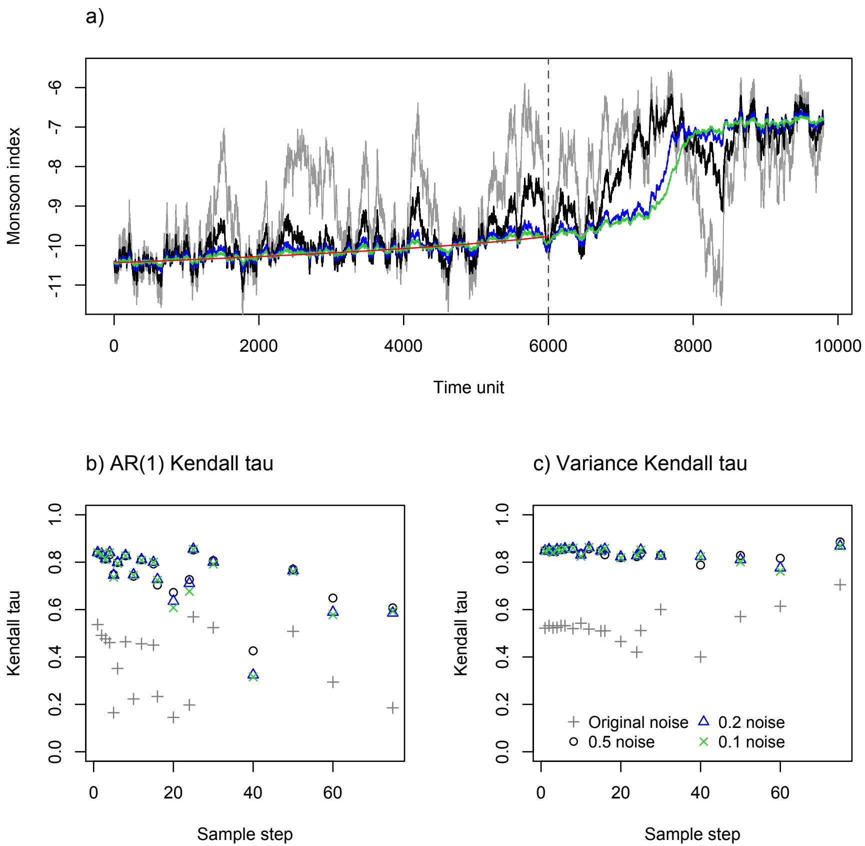

Figure 12. (a) Example of single realisation of the approach to a bifurcation over 4 noise levels (original noise = grey, 0.5 noise = black, 0.2 noise = blue, 0.1 noise = green), red line is the detrending line and the grey dashed vertical line is the cut-off point where data is analysed up to; **(b)** distribution of Kendall Tau values for AR(1) over increasing sample step; **(c)** distribution of Kendall Tau values for variance over increasing sample step.

CPD
11, 1313–1341, 2015